Proceedings of the 5th WSEAS Int. Conf. on Signal Processing, Computational Geometry & Artificial Vision, Malta, September 15-17, 2005 (pp77-81)

Wavelet-based Deconvolution Algorithms Applied to Ultrasound Images

S. Maggio, N. Testoni, L. De Marchi, N. Speciale and G. Masetti
Department of Electronics, Informatics and Systems
University of Bologna
V.le Risorgimento 2, Bologna, Italy

Abstract: - Since deconvolution is a recurring theme in a wide variety of signal and image processing applications, many algorithms have been proposed to address this problem. In particular, in ultrasound imaging, deconvolution is often applied as a fundamental step either for contrast enhancement or as preprocessing in segmentation procedures. In this work we present a comparative study between two wavelet-based deconvolution algorithms as tools for processing ultrasound images, one based on a minimization of an error energy term, the other performing a two-step regularization procedure on both the Fourier and Wavelet domain. The comparison is made in terms of Mean Square Error (MSE) and Signal to Noise Ratio (SNR) calculated on synthetic signals. Moreover, we estimate the computational cost and we provide processed B-mode images through which background noise smoothing and edge sharpness enhancement could be qualitatively evaluated.

Key-Words: - Wavelet, Deconvolution, Ultrasound, Least Square, Fourier Transform.

1 Introduction

Ultrasound images are extensively used as a diagnostic instrument in many fields, especially in medicine [1, 2, 3]. As the ultrasound transducer introduces an unwanted spectral shaping of the backscattered echo signal, deconvolution is used to eliminate this effect and to obtain the pure tissue response. A convenient model to represent RF echo signal $y(n)$ at the transducer output involve the convolution between the tissue reflectivity function $x(n)$ and the transducer impulse response $g(n)$:

$$y(n) = x(n) * g(n) + \gamma(n) \tag{1}$$

were $\gamma(n)$ is a zero-mean additive Gaussian noise (AWGN) term with variance σ^2 [7] and $*$ denotes the the convolution operation. Given $y(n)$ and $g(n)$, deconvolution algorithms seek to estimate $x(n)$. A naïve deconvolution estimate $\hat{x}(n)$ can be obtained by simply convolving $y(n)$ with an approximation of the inverse transducer impulse response $\hat{w}(n)$ so that

$$g(n) * \hat{w}(n) = \delta(n - n_0)$$

and

$$\hat{x}(n) = x(n - n_0) + \gamma(n) * \hat{w}(n) \tag{2}$$

where $\delta(n)$ is the Kronecker delta function and n_0 is the time-delay when the impulse response is non-minimum phase. Unfortunately, the variance of the colored noise $\gamma(n) * \hat{w}(n)$ in $\hat{x}(n)$ is large when the inversion process involving $g(n)$ is ill conditioned as well as the Mean Square Error (MSE) between $\hat{x}(n)$ and $x(n)$, making $\hat{x}(n)$ an unsatisfactory deconvolution estimate. In general, deconvolution algorithms can be interpreted as estimators of $x(n)$ from the noisy signal $\hat{x}(n)$ in (2).

The presented deconvolution algorithms exploit the fact that the tissue response $x(n)$ can be *economically* represented in the Wavelet domain, which means that fewer transform-domain coefficients are needed to capture signal features. From another standpoint, the tissue response $x(n)$ can be modeled as a $1/f$ type process due to the complex structure of the echo scatterers in the tissue [10]; the generalized power spectrum $S_x(\omega)$ of such a process obeys a to the following power law [9, 11]

$$S_x(\omega) = \sigma_x^2 |\omega|^{\beta - 1} \tag{3}$$

where σ_x^2 is the variance of the signal $x(n)$ and β is a scaling parameter in the range $-1 \leq \beta \leq 1$. Using this model, the variance of the Wavelet signal coefficients $x_j(n)$ can be shown to be

$$\mathrm{var}\{x_j(n)\} = \sigma_w^2 2^{-j\beta} \tag{4}$$

where j is the scale index and σ_w^2 a constant related to the variance of the signal σ_x^2 and the Wavelet function used in the Wavelet Decomposition process [10]. By taking the logarithm of (4), a linear relationship between the Wavelet scale and the logarithm of the variance of input signal Wavelet coefficients is obtained. This relationship can be exploited to improve the estimate of the tissue response $x(n)$.

In the following sections we summarize the main features of the considered algorithms.

2 Wavelet Domain Least Squares Deconvolution

The Wavelet Domain Least Squares Deconvolution algorithm (WLSD) [5] uses equation (4) to drive a gradient

based optimization technique, minimizing an error energy term ϵ. Starting from the Wavelet series $X_j(k)$ of the discrete-time signal $x(n)$, the Wavelet coefficients at each scale j can be written in the matrix and vector notation as

$$\mathbf{X}_j = \mathbf{H}_j \mathbf{x}, \qquad j = 1, \ldots, J \tag{5}$$

where $\mathbf{H}_j$ is a convolution type matrix whose elements corresponds to the equivalent filter coefficients for the j-th scale, $\mathbf{x}$ is the signal vector and J is the total number of scales. In absence of noise ($\gamma(n) = 0$) the Wavelet coefficients $\hat{\mathbf{X}}_j$ at each scale of the approximative tissue response estimate $\hat{x}$ can be expressed in function of known parameters:

$$\hat{\mathbf{X}}_j = \mathbf{D}_j \hat{\mathbf{w}}, \qquad j = 1, \ldots, J \tag{6}$$

where $\mathbf{D}_j$ is a matrix dependent on $\mathbf{H}_j$ and on observation y, while $\hat{\mathbf{w}}$ is the approximation of the inverse filter vector.

The most important task in determining the energy error is computing variance V_j of Wavelet coefficients $\hat{\mathbf{X}}_j$ at the j-th scale:

$$V_j = \frac{\hat{\mathbf{X}}_j^T \hat{\mathbf{X}}_j}{N_j - 1} = \frac{\hat{\mathbf{w}}^T \mathbf{D}_j^T \mathbf{D}_j \hat{\mathbf{w}}}{N_j - 1} = \hat{\mathbf{w}}^T \mathbf{C}_j \hat{\mathbf{w}} \tag{7}$$

where N_j is the number of Wavelet coefficients at the j-th scale.

The energy error depends on the difference from linearity of the logarithmic variance progression at each scale of the Wavelet Transform together with the difference from an impulsive function of the convolution of the estimated inverse filter with the transducer impulse response:

$$\begin{aligned} \epsilon(\hat{\mathbf{w}}, \hat{\alpha}, \hat{\beta}) \quad = \quad & \sum_{j=1}^{J} \Big(\log_2(\hat{\mathbf{w}}^T \mathbf{C}_j \hat{\mathbf{w}}) - (\hat{\alpha} - j\hat{\beta}) \Big)^2 + \\ & + (\mathbf{G}\hat{\mathbf{w}} - \delta)^T (\mathbf{G}\hat{\mathbf{w}} - \delta) \end{aligned} \tag{8}$$

In this formula $\hat{\beta}$ and $\hat{\alpha}$ are the estimates of the scaling parameter and of the energy parameter $\alpha = \log_2(\sigma_w^2)$ respectively, and $\mathbf{G}$ is the convolution matrix for the transducer impulse response and $\delta = [0 \ldots 0\, 1\, 0 \ldots 0]^T$. The energy error is used to drive an iterative minimization technique based on the conjugate gradient. In order to speed-up algorithm convergence, the gradient and the Hessian matrix of the error energy $\epsilon(\hat{\mathbf{w}}, \hat{\alpha}, \hat{\beta})$ should be obtained algebrically; additionally, *ad-hoc* proconditioners can be used to further reduce the estimation time. Good guess for the first iteration are $\hat{\mathbf{w}} = \mathbf{G}^{\dagger}\delta$, $\hat{\alpha} = 0$ and $\hat{\beta} = 0$.

This algortithm gives really good results whenever the white gaussian noise $\gamma(n)$ in the model (1) is negligible when compared to the tissue impulse response $x(n)$.

3 Fourier-Wavelet Regularized Deconvolution

The Fourier-Wavelet Regularized Deconvolution algorithm (FWRD) [4] consider the RF echo transducer as a linear time-invariant system $\mathcal{H}$ whose impulse response, accordingly to (1), is $g(n)$. Scalar shrinkage is used in both Fourier and Wavelet domains to obtain a good estimation of $x(n)$ from $\hat{x}(n)$: this double-domain technique allows for an optimized representation of both the input signal $x(n)$ and the contaminating noise $\gamma(n)$, since $x(n)$ is better represented in the Wavelet domain while $\gamma(n)$ in the Fourier domain.

Given an orthonormal (Fourier or Wavelet) basis $\{b_k\}_{k=0}^{N-1}$ for $\mathbb{R}^N$, $\hat{x}$ from (2) can be expressed as

$$\hat{x} = \sum_{k=0}^{N-1} \big(\langle x, b_k \rangle + \langle \hat{w} * \gamma, b_k \rangle \big) b_k \tag{9}$$

where $\hat{w}$ is again the inverse transducer impulse response. An improved estimate $\hat{x}_\lambda$ can be obtained by simply shrinking the k-th component in (9) with an appropriate scalar λ_k with $0 \leq \lambda_k \leq 1$:

$$\hat{x}_\lambda = \sum_{k=0}^{N-1} \big(\langle x, b_k \rangle + \langle \hat{w} * \gamma, b_k \rangle \big) \lambda_k b_k \tag{10}$$

The parameter λ_k should be taken close to 1 whenever noise energy is negligible compared to signal energy, and close to 0 in the reciprocal case. The shrinkage by λ_k can also be interpreted as a form of regularization for the deconvolution inverse problem [12].

In the Fourier domain, model (1) can be written as

$$Y(f_k) = H(f_k) X(f_k) + \Gamma(f_k) \tag{11}$$

where Y, H, X and Γ are the N-length Discrete Fourier Transform (DFT) of y, h, x and γ respectively, while $f_k = \pi k/N$, $k = 1, \ldots, N$ are the normalized DFT frequencies. Rewriting (2) in the Fourier domain we obtain

$$\hat{X}(f_k) = X(f_k) + \frac{\Gamma(f_k)}{H(f_k)} = \frac{Y(f_k)}{H(f_k)} \tag{12}$$

and the DFT $\hat{X}_{\lambda f}(f_k)$ of the Fourier shrinked estimate can be written as

$$\hat{X}_{\lambda f}(f_k) = \frac{Y(f_k) H^*(f_k)}{|H(f_k)|^2 + \tau} \tag{13}$$

where $\tau > 0$ is a regularization parameter which can be optimized in order to minimize the Mean Square Error (MSE) between the tissue reflectivity function $x(n)$ and its final estimate $\hat{x}(n)$ after both Fourier and Wavelet shrinking have been applied [14]. Since in real cases $x(n)$ is not available, τ is set to minimize the MSE between $y(n)$ and its estimate $\hat{y}(n)$ generated from $\hat{x}(n)$.

The following Wavelet shrinking process involves the Discrete Wavelet Transform (DWT) of the signal $\hat{x}_{\lambda f}(n)$ obtained from the inverse DFT of $\hat{X}_{\lambda f}(f_k)$. The final estimate $\hat{x}(n)$ is obtained by applying the Inverse DWT to the shrinked Wavelet and scaling coefficients.

Original		**WLSD**		**FWRD**	
N_x	SNR	SNR	MSE	SNR	MSE
64	80	58.42	$1.796 \cdot 10^{-6}$	12.22	0.074775
64	50	30.31	0.0011611	12.2	0.075197
64	20	-2.61	2.2753	10.81	0.10346
128	80	51.32	$3.3274 \cdot 10^{-6}$	14.78	0.015
128	50	24.43	0.00163	14.64	0.015499
128	20	-7.89	2.7743	8.91	0.058007
256	80	51.03	$9.0354 \cdot 10^{-6}$	21.98	0.0072612
256	50	26.93	0.0023203	21.65	0.0078378
256	20	-5.54	4.0977	11.23	0.086277

Table 1: Comparison between WLSD and FWRD: WLSD performs better in low noise environments, while FWRD gives more accurate results when noise is higher.

4 Comparison between WLSD and FWRD algorithms

Implementation of both WLSD and FWRD algorithm have been tested on simulated $1/f$ signals, convolved with a typical trasducer impulsive response and corrupted with additive white Gaussian noise. For all signals the effect of length and initial SNR have been tested. The obtained estimates $\hat{x}(n)$ have been compared to original signals $x(n)$, by measuring final SNR and MSE:

$$\begin{aligned} \mathrm{SNR} &= 10 \log_{10} \left(\frac{\|x\|^2}{\|\hat{x} - x\|^2} \right) \mathrm{dB} \\ \mathrm{MSE} &= \mathbb{E}(|\hat{x} - x|^2) \end{aligned} \tag{14}$$

In the next subsections, some important differences between WLSD and FWRD and the computational cost of the two algorithms are shown.

4.1 Simulations Results

The comparison between FWRD and WLSD was made evaluating the deconvolution performance on different $1/f$ signals, with number of sample 64, 128 and 256 and with different SNR, from 20 to 80 dB. Simulation results, summarized in Tab. 1, show that in presence of low noise, WLSD provides more precise estimates than FWRD and produces an excellent tissue response reconstruction with a very low MSE. On the contrary, when noise is large (SNR<30 dB), WLSD fails in recovering the original signal, while FWRD is able to reconstruct the shape of the tissue response, although it yields less exact estimates than the previous case.

An example is shown on Fig. 1 where a 128 samples $1/f$ signal, its corresponding observation with $\mathrm{SNR} = 80$ dB and WLSD and FWRD deconvolution results are plotted. In Fig. 2 the same original signal and observation with $\mathrm{SNR} = 20$ dB is shown. In this case the failure of WLSD deconvolution is evident.

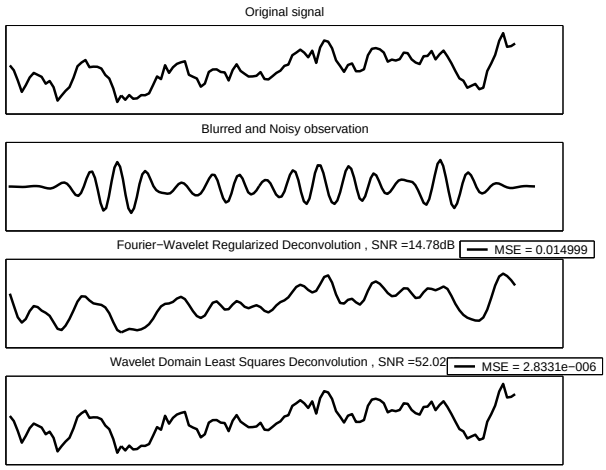

Figure 1: Deconvolution of an high SNR blurred and noisy observation: WLSD performs better than FWRD, achieving an MSE lower than $3 \cdot 10^{-6}$ and an SNR higher than 50 dB.

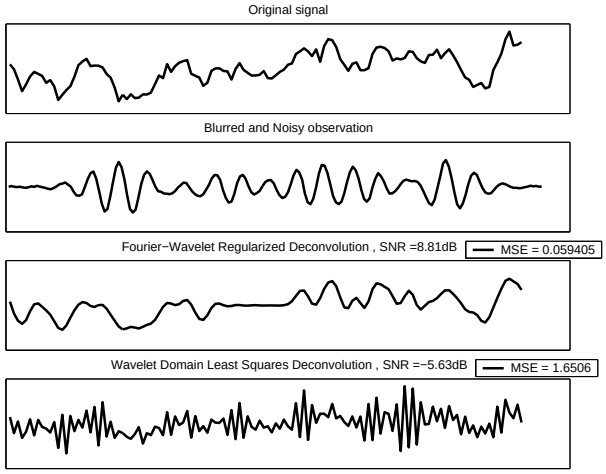

Figure 2: Deconvolution of a low SNR blurred and noisy observation: FWRD performs better than WLSD, achieving an MSE lower than $6 \cdot 10^{-2}$ and an SNR higher than 8 dB.

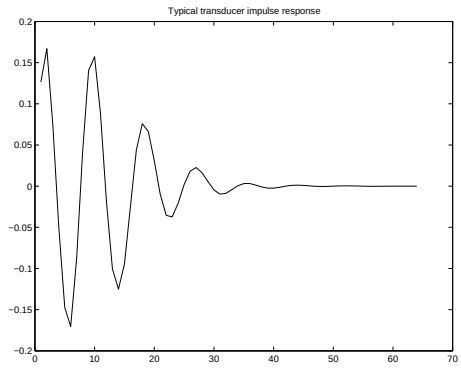

Figure 3: Estimated transducer pulse used in both deconvolution algorithms

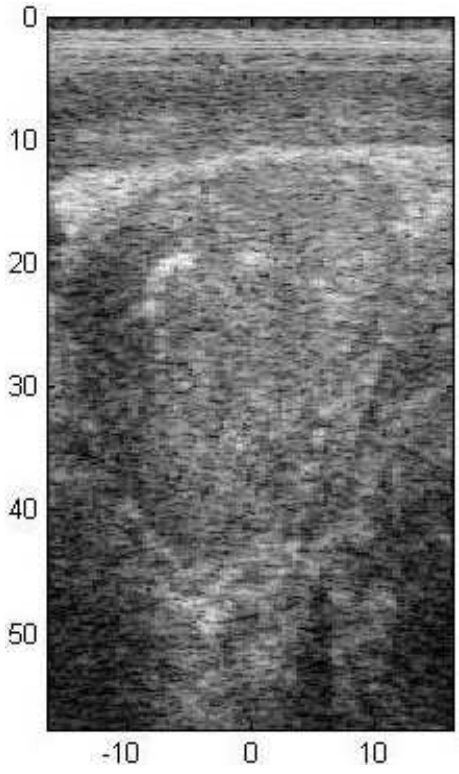

Figure 4: In-vivo image of a prostatig gland affected by carcinoma; the unhealty zone is visible in the left side of the image.

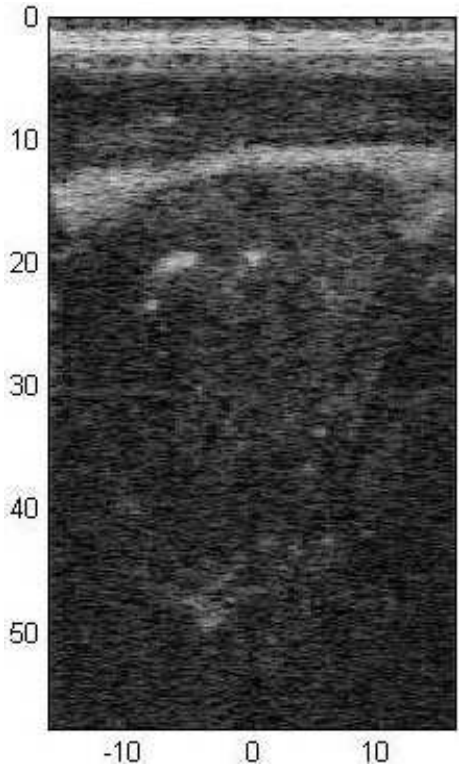

Figure 5: WLSD processed in-vivo image: global contrast is still better than the original image, however the unealthy zone is less evident.

4.2 Computational Cost

Both the algorithms rely on the multiresolution properties of the Wavelet Transform whose computation is very efficient: for discrete-time signals with N samples, the N Wavelet coefficients can be computed in $O(N)$ operations using a filterbank consisting of lowpass filters, highpass filters, upsamplers and decimators [13].

WLSD is composed of an initialization part in which the calculation of $\mathbf{D}_j$ and $\mathbf{C}_j$ is performed. Such task is quite honerous and depends on the inverse filter length N_w, on the observed signal length N_y and on the trasducer response length N_h linearly. Instead, in WLSD iterations, gradient and Hessian matrix computation are the most time consuming operations. The computational cost of WLSD algorithm could be extimated by the following expression:

$$O((N_w + N_y)^3 \log_2(N_y)) \tag{15}$$

As regards FWRD algorithm the most honerous operations are FFT and IFFT calculation, which only depend on the observed signal length. Consequently the computational cost of FWRD algorithm has the following expression:

$$O(N_y \log_2(N_y)) \tag{16}$$

As a consequence FWRD algorithm is less sensitive than WLSD to an increase of N_y.

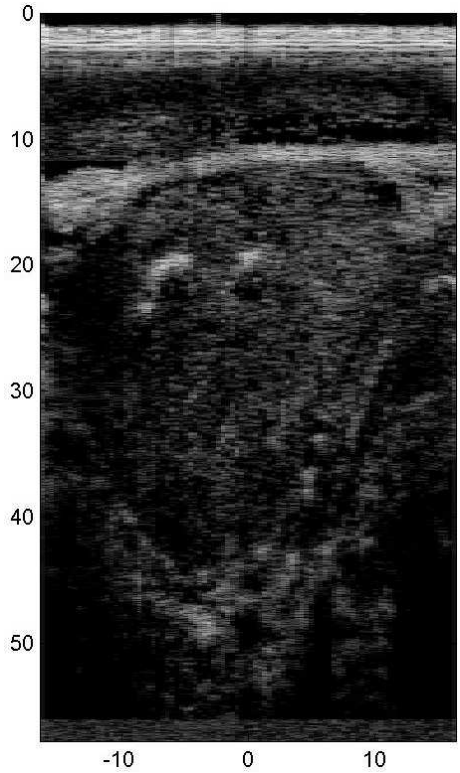

Figure 6: FWRD processed in-vivo image: global contrast is better than the original image and the unealthy zone can be seen more clearly.

5 Conclusions

To qualitatively evaluate the performance of the algorithms, we considered a real ultrasound image. Fig. 4 shows a prostate affected by carcinoma. The noisy image is acquired in-vivo. On this image we have applied both the algorithms estimating the transducer pulse (see Fig. 3) with an approach based on the modification of the homomorphic deconvolution described in [15].

WLSD (Fig. 5) seems not adequate to enhance the ultrasound image quality, because the large presence of noise in images acquisition compromises deconvolution capability. In contrast FWRD (Fig. 6) is a good tool to deblur and denoise ultrasound images, and it allows for an accurate identification of the ipoechogenic pathological tissue on the left side of the prostatic gland. However, when processing echo images, FWRD displays a greater computational cost than WLSD due to the image reconstruction procedure adopted.

In fact, the use of one-dimensional algorithms on images needs preliminary segmentation followed by image reconstruction. Each tissue responds to ultrasound with different signal intensity, thus generating regions with different brightness in echo images. This feature is used by Wavelet-based algorithms in order to operate images enhancement. Finally, visual quality provided by FWRD could be used to identify biological tissues and separate healthy and unhealthy regions for diagnostic purposes.

References

[1] M.F. Insana, R.F. Wagner, D.G. Brown, T.J. Hall, "Describing small-scale structure in random media using pulse-echo ultrasound", *J. Acoust. Soc. Amer.*, vol. 87, pp. 179-192, Gen. 1990

[2] M.F. Insana, T.J. Hall, "Characterizing the microstructure of random media using ultrasound", *Phys. Med. Biol.*, vol. 35, pp. 1373-1386, Ott. 1990

[3] J.A. Jensen, "Ultrasound imaging and its modeling", *Imaging of Complex Media with Acoustic and Seismic Waves*, ed. Springer Verlag, 2000

[4] R. Neelamani, H. Choi, R. Baraniuk, "ForWaRD: Fourier-Wavelet Regularized Deconvolution for Ill-Conditioned Systems", *IEEE Trans. on signal processing*, vol.52, NO.2, February 2004.

[5] M. Izzetoğlu, B. Onaral, N. Bilgütay, "Wavelet Domain Least Squares Deconvolution for Ultrasonic Backscattered Signals", *Proceedings of the* 22^{nd} *Annual EMBS International Conference*, July 23-28, 2000, Chicago.

[6] D. G. Luenberger, *Introduction to Linear and Nonlinear Programming*, Addison-Wesley, 1973.

[7] D. L. Donoho,"De-Noising by Soft Thresholding", *IEEE Trans. Inform. Theory*, vol.41, NO.3, May 1995.

[8] D. L. Donoho, I. M. Johnstone, "Threshold selection for wavelet shrinkage of noisy data", *IEEE*, 0-7803-2050-6D4, 1994.

[9] A Van Der Ziel, "Unified Presentation of $1/f$ Noise Sources", *Proc.IEEE*, Vol.76, pp.233-258, 1988.

[10] G. W. Wornell, *Signal Processing with Fractals: A Wavelet-Based Approach*, Prentice Hall, 1996.

[11] G. W. Wornell, "A Karhunen-Love-like Expansion for $1/f$ Processes via Wavelets", *IEEE Trans. in Information Theory*, Vol.36, pp.859-861, 1990.

[12] A. K. Katsaggelos, Ed., *Digital Image Restoration*. New York: Springer-Verlag, 1991.

[13] S. Mallat, *A Wavelet Tour of Signal Processing*. New York: Academic, 1998.

[14] A. N. Tikhonov, V. Y. Arsenin, *Solutions of Ill-Posed Problems*. Washington, DC: Winston, 1977.

[15] D. Adam, O. Michailovich, "Blind Deconvolution of Ultrasound Sequences Using Nonparametric Local Polynomial Estimates of the Pulse", *IEEE Trans. on Biomedical Engineering*. Vol.49, No.2, Febbruary 2002.